DOI: 10.1002/ejic.200900369

Facile Synthesis of Anatase–Brookite Mixed-Phase N-Doped TiO_2 Nanoparticles with High Visible-Light Photocatalytic Activity

Li Li[a,b] and Chun-yan Liu*[a]

Keywords: Titanium / Solvothermal synthesis / Photochemistry / Doping

N-Doped anatase–brookite bicrystal TiO_2 nanocatalysts were successfully synthesized by a facile solvothermal route. The ratio of brookite to anatase can be easily tuned by changing the composition of the phase-selective agents (acetylacetone). The samples were fully characterized. The band-gap energy, chemical states of Ti, O, and N species, and photocatalytic activity of the as-prepared catalysts were affected by the mixed-phase effect of brookite and anatase. In the optimum ratio range of the phase effect from 24.6 to 75.4 % (brookite to anatase), the N-doped TiO_2 bicrystal catalyst exhibits maximum activity under both visible and UV light, which can be attributed to high quantum efficiency induced by the high concentration of $OH_{surface}$, the relatively low amount of Ti^{3+} sites, active N^- species concentration, the relatively large surface areas, and a moderate band-gap energy.

Introduction

Research on the design and controlled synthesis of titanium dioxide (TiO_2) has attracted considerable attention in the past decades[1,2] because of its excellent photocatalytic capability in degrading a large variety of environmental contaminants such as organic materials, bacteria, and viruses,[3,4] especially after the discovery of photoinduced water-splitting by TiO_2.[5] However, in most cases, UV light is needed when TiO_2 is used as a photocatalyst because of its large band-gap energy (3.2 eV for anatase TiO_2). Therefore, they are not suitable for some important applications that require easily activated photocatalysts with low band-gap energies, such as daylight-induced chemical reactions. In addition to its large band-gap energy, the low quantum efficiency of TiO_2 also limits its application. Currently, it is still of great importance to explore facile and reliable means aiming at TiO_2 materials with improved catalytic performances (including the spectral response range and the quantum efficiency) in order to be used in a broader spectrum range more efficiently.[6–8]

A photocatalyst with a high reactivity under visible light ($\lambda > 380$ nm) can utilize the main part of the solar spectrum, and even poor illumination of interior lighting. Till now, many studies have been attributed to the doping of TiO_2 with transition-metal elements to enlarge its visible spectral response.[9–12] However, transition-metal-doped TiO_2 always suffers from an increase in carrier-recombination centers and a decrease in photocatalytic activity under ultraviolet light.[13] An alternative way to extend the light response range is to use a nonmetallic doping element. Since the first synthesis of an N-doped TiO_2 visible-light photocatalyst by Asahi in 2001,[14] the modification of TiO_2 with N dopants seems a powerful way to extend the absorption light from the UV area to the visible area, because the substitution of lattice oxygen with nitrogen can narrow the band gap by mixing the N_{1S} and O_{1S} states,[15–17] and this avoids increased recombination centers given by the localized d states of the cationic metals. However, the practical application of N-doped titania is still hindered by its low reactivity and quantum efficiency.[18] Further, up to now, almost all N-doped TiO_2 samples are prepared by treating TiO_2 under an NH_3 atmosphere at high temperature. The process is highly energy consuming and treatment at high temperature usually results in low reactivity as a result of the low surface area caused by agglomeration and decreased hydroxy group concentration on the surface of the catalysts.[18]

As for the enhancement in the quantum efficiency of TiO_2, there are three strategies commonly used: noble metal deposition, coupling with other narrow band-gap semiconductors, and phase mixing.[19,20] Among the three strategies, phase mixing is the most promising; a typical example is commercial Degussa P25, an anatase–rutile mixed-phase catalyst. With anatase as an active component and rutile as an electron sink[21a,21b] (under visible illumination, the process of electron transfer from rutile to anatase lattice trap-

[a] Key Laboratory of Photochemical Conversion and Optoelectronic Materials Technical Institute of Physics and Chemistry, Chinese Academy of Sciences,
Beijing 100190, P. R. China
Fax: +86-10-62554670
E-mail: cyliu@mail.ipc.ac.cn
[b] College of Chemistry and Chemical Engineering, Graduate School of the Chinese Academy of Sciences
Beijing 100806, P. R. China

Supporting information for this article is available on the WWW under http://dx.doi.org/10.1002/ejic.200900369.

ping sites can also occur[21c]), P25 shows slower rates of recombination and thus higher photocatalytic activity than its pure phase counterparts.

Among the three crystalline phases of TiO_2 (anatase, rutile, and brookite), anatase generally shows better performances than its rutile counterpart in photocatalytic applications.[6,22] The brookite phase is the least studied in many aspects of its properties, mainly owing to the difficulties in preparation, though it seems to have some special properties, like the marked photocatalytic activity (comparable to anatase) in the dehydrogenation of propan-2-ol and in Ag deposition.[23] Whereupon, the controlled synthesis and study of the mixed crystal effect of the brookite and other TiO_2 phases will open a new millennium for the development of mixed-phase catalysts.

In our work, anatase–brookite bicrystal N-doped TiO_2 was designed and synthesized by a facile solvothermal method. The modification of TiO_2 with N dopants was used to narrow the band gap and extend the absorption from UV to visible light. The mixing of anatase and brookite was designed to enhance the quantum efficiency of the N-doped TiO_2 samples. It is found that the ratio of brookite to anatase can be easily tuned by changing the composition in an initial solution. The band-gap energy of N-doped TiO_2, chemical states of Ti, O, and N species on the surface have been proved to be affected by the mixed-phase effect of brookite and anatase. At the optimum ratio of brookite to anatase (24.6 to 75.4%), the N-doped TiO_2 bicrystal catalyst exhibits maximum activity both under visible and UV light, which shows the same high activity as P25.

Results and Discussion

To determine the phase contents, all samples were examined by XRD (Figure 1). Figure 1a shows the pure anatase sample prepared by solvothermal treatment of the tetrabutyltitanate–DMF system. When acetylacetone was added to the reaction system (Kominami et al. reported the preparation of brookite TiO_2 by using titanium acetylacetonate as a titanium source.[24] Hence, it suggests that acetylacetone can be used as a phase-selective agent to produce the brookite phase through the formation of titanium acetylacetonate in the reaction system), anatase–brookite mixed-crystal samples were obtained (Figure 1b–e). The calculated ratios of brookite to anatase in the sample (Table 1) indicate that the brookite component increases along with the concentration of acetylacetone used. The crystal phase compositions and the crystal sizes of the samples are listed in Table 1. It can be seen that with an increased content of a certain phase, the corresponding size of the crystallites of this phase increases gradually.

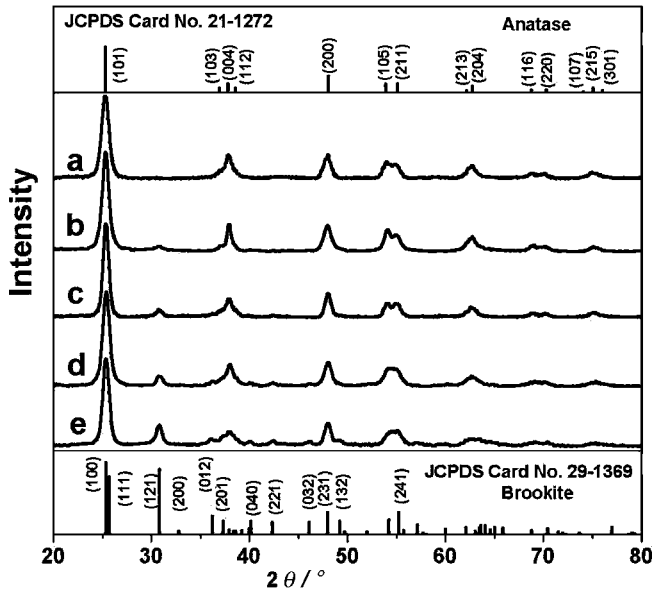

Figure 1. XRD patterns of the as-obtained products in Table 1.

The surface states of the N-doped TiO_2 samples were investigated by XPS, and the data listed in Table 2. Figure 2-1 shows the XPS spectra for the N_{1s} region of N-doped TiO_2 with different ratios of brookite to anatase. A broad peak from the binding energy region 397–404 eV is observed for each sample. Three binding energy regions centered at 400, 401, and 402 eV are obtained through curve fitting. All the five characteristic peaks can be steadily indexed to NO and Ti–O–N, O–Ti–N linkages, which are the typical of N species in the TiO_2 lattice.[25] These results clearly demonstrate that through solvothermal treatment of the tetrabutyltitanate DMF solution, the N-doped TiO_2 catalysts were obtained successfully. In light of doping with NH_3 as a dopant, Scheme 1 briefly describes the possible nitridation process.

In the beginning, DMF can hydrolyze to generate $NH(CH_3)_2$ and HCOOH in the presence of a trace amount of water [adsorbed water of $Ti(OC_4H_9)_4$, acac, and DMF; step 1].[26] This hydrolysis process can be confirmed by the

Table 1. Experimental conditions and parameters of the catalyst.

Sample	Amounts of chemicals / mL			Relative phase content / %		Crystallite size / nm		Optical band gap energy / eV	Particle size / nm	BET surface area / m^2g^{-1}
	$Ti(OC_4H_9)_4$	DMF	ACAC	brookite	anatase	brookite	anatase			
a	1.5	25	0	0	100	0	19.6	2.81	21	76.0
b	1.5	25	1	10.9	89.1	8.6	11.3	2.91	21	72.5
c	1.5	25	3	24.6	75.4	10.7	9.8	2.92	22	76.2
d	1.5	25	5	29.8	70.2	10.9	9.6	2.94	21	78.0
e	1.5	25	7	48.4	51.6	11.0	9.5	2.97	22	76.5
P25	–	–	–	–	–	–	–	3.02	–	50.0

Table 2. XPS data of N, O, and Ti.

Sample	Atom ratio of O/Ti/N	Relative contents of the elements in the sample per atom / %							
		O		Ti		N			
		$OH_{surface}$	$O_{lattice}$	Ti^{3+}	Ti^{4+}	–N^-	–NO	Ti-O–N	O–Ti–N
a	57.17:20.03:0.08	12.3	87.7	10.2	89.8	0	56.8	2.9	40.3
b	67.65:20.02:0.08	32.2	67.8	2.8	97.2	13.4	55.1	20.5	11.0
c	67.57:18.19:0.07	39.8	60.2	2.3	97.7	29.8	30.4	6.1	33.7
d	64.31:17.52:0.07	37.3	62.7	1.1	98.9	17.1	45.9	5.4	31.6
e	59.27:20.03:0.08	12.5	87.5	0.1	99.9	0	74.3	20.8	4.9

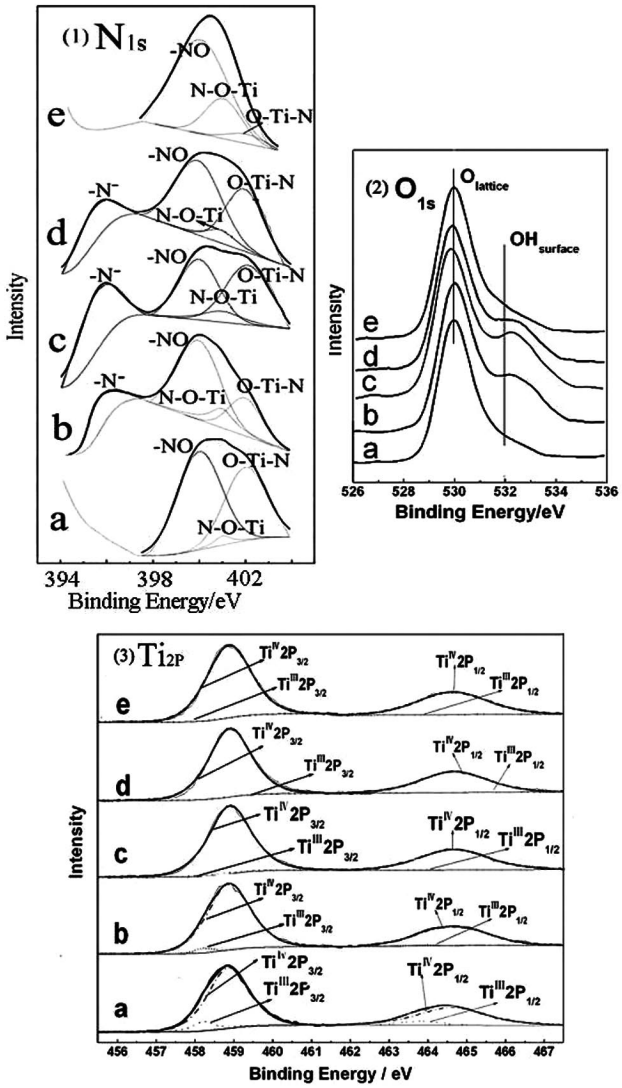

Figure 2. High-resolution XPS analysis of N-doped TiO_2 samples in Table 1: (1) N_{1s} region, (2) O_{1s} region, and (3) Ti_{2p} region.

intense amine odor from the solution after the reaction. Step 2 is the surface adsorption of $NH(CH_3)_2$ molecules onto the nascent TiO_2 networks. Subsequently, the nitrogen atom in $NH(CH_3)_2$ dopes into the TiO_2 lattice by the formation of the O–Ti–N and Ti–O–N species, as illustrated in steps 3 and 4. A similar mechanism was reported with NH_3 as a dopant.[18] Another peak centered at a lower binding energy (396 eV) is attributed to a chemically

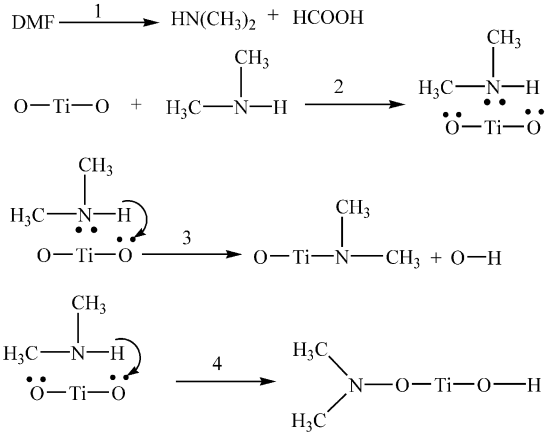

Scheme 1. Formation of O–Ti–N and Ti–O–N nitrides.

bonded N-species within the TiO_2 lattice. Following Asahi, the peak at 396 eV is the active site and related enhanced photocatalytic activity.[14] This signal cannot be observed for samples with a too high (48.1%) or too low (0%) brookite content. For the other three bicrystal N-doped TiO_2 samples, the intensity of this peak follows the order c > d > b (Figure 2-1).

As shown in Table 2, the ratio of the N species maintained in N-doped TiO_2 varies with changes in the phase composition in the catalysts, indicating that the mixing of brookite with anatase severely affects the chemical states of the doped N. Moreover, all the as-prepared catalysts contain a similar total N amount by XPS investigation, which clearly reveals that the brookite content in the samples has little influence on the concentration of the doped N.

Figure 2-2 shows the XPS spectra of the O_{1s} region. Generally, the photoelectron peaks of O_{1s} can be curve fitted at about 529.9, 531.9, and 533.4 eV, which correspond to the titania lattices, surface hydroxy groups, and adsorbed oxygen mainly from adsorbed water molecules.[27,28] This figure also illuminates that the quantity of the adsorbed oxygen on the surface of the N-doped TiO_2 samples could be neglected, the mixing of brookite and anatase increases the concentration of the surface hydroxy groups, and the sequence of the surface hydroxy concentration for the five samples is c > b > d >> e ≈ a. As has been previously reported, several factors, including the crystal phase, properties of external crystal planes, the absorbed H_2O, may have various effects on the surface OH distribution.[29] In present work, it is found that the $OH_{surface}$ concentration changes with the ratio of anatase to brookite. The reason

may be with reference to the alternation of the properties of external surface crystal planes induced by the variation of the phase ratio. However, more in-depth study is still needed to further understand the effects of the anatase–brookite ratio on the surface OH concentration.

The binding energy at 458.8 and 464.6 eV can be attributed to the $Ti_{2p3/2}$ and $Ti_{2p1/2}$ core levels of the N-doped TiO_2 samples, respectively (Figure 2-3).[30] There is no apparent change in the Ti_{2p} peak position for all the samples. According to the 0.7 eV ($Ti_{2p3/2}$) and 0.8 eV ($Ti_{2p1/2}$) negative shift of the chemical state of Ti^{4+} and Ti^{3+}, respectively, the chemical states of titanium (Ti^{4+} and Ti^{3+}) are analyzed in detail by deconvolution by using Gaussian mixture peak fitting.[31] As shown in Table 1, compared with the pure anatase N-doped TiO_2, the concentrations of the Ti^{3+} sites on the surface of bicrystal N-doped TiO_2 catalysts are much lower.

As shown in Figure 3, the shoulder of the absorption spectrum of N-doped TiO_2 samples are significantly extended toward the visible light range, possibly owing to the substitution of the lattice oxygen by nitrogen during TiO_2 nitridation. This is of great importance for the application of N-doped TiO_2 materials, as they can be activated even by sunlight. The relative band-gap energies of the as-prepared samples and P25 are shown in Table 1. The N-doped TiO_2 sample possesses a narrower band gap than P25 owing to the mixing of the N_{1S} and the O_{1S} states.[32] It is interesting that with an increase in the brookite content in the N-doped products (from 0 to 48.4%), the band gap energies widen from 2.81 to 2.97 eV. This may probably be attributed to the decreased concentration of the Ti^{3+} states, which has been found to be below the bottom of the conduction band.[33] In Figure 3, the as-prepared samples have larger background signals than P25. This may be caused by nitrogen doping and aggregation of the product particle induced by the post-treating process (the presence of the large aggregates are confirmed by SEM observation of the synthesized materials, see Figure S1).

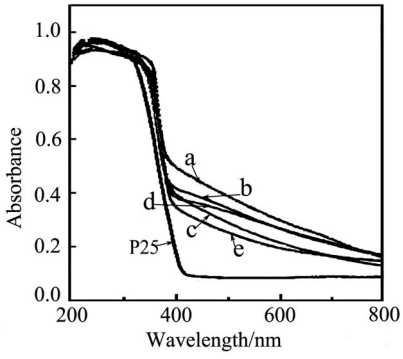

Figure 3. UV/Vis diffusive reflectance spectra of the samples in Table 1 and P25.

The TEM images of the as-obtained samples are shown in Figure 4. It can be seen that all of the five samples consist mainly of ca. 20 nm nanoparticles, and the changing phase composition has little influence on the morphology of the products. In addition, the Brunauer–Emmett–Teller (BET) surface areas of the as-prepared samples are measured by nitrogen adsorption. The data are listed in Table 1. It can be seen that all five samples have similar surface areas that are higher than that of P25 ($50\ m^2\,g^{-1}$),[34] which will be favorable to their photocatalytic activities.

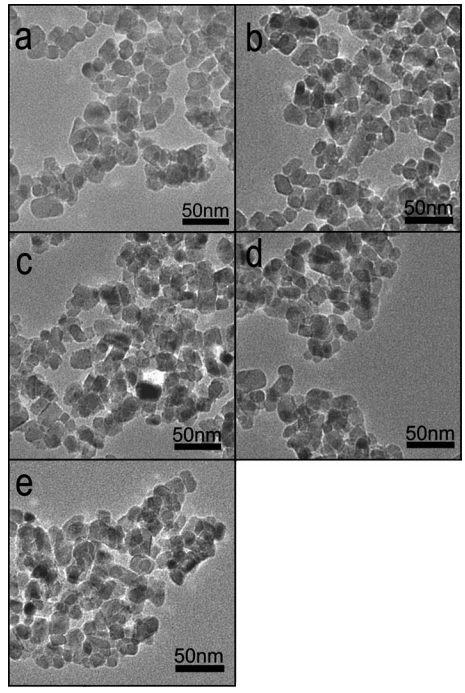

Figure 4. TEM images of N-doped TiO_2 in Table 1.

Methylene blue (MB) is often selected as a model pollutant for photocatalytic oxidation experiments, because it is a common toxic azo dye in colored wastewater. Figure 5 describes the activity of as-prepared N-doped TiO_2 samples under visible and UV light, where C and C_0 stand for the remnant and initial concentration of MB, respectively. In the visible-light region (Figure 5A), the N-doped samples possess better photocatalytic activities than P25. The degradation rate of MB on different TiO_2 catalyst samples under visible light irradiation follows the order: c > d > b > a > e >> P25. In contrast, the phase mixing also can remarkably improve the UV-photocatalytic activities of N-doped samples. As shown in Figure 5B, with a properly controlled phase composition, N-doped TiO_2 catalysts exhibit a comparable photocatalytic activity to Degussa P25. The degradation rate of MB on different TiO_2 catalyst samples under UV irradiation follows the order: c = P25 > d > b > e > a.

As is well known, the quantum efficiency affects activities of the photocatalysts significantly,[6] and to monitor the surface properties is an effective strategy to adjust the quantum efficiency. One way to enhance the quantum efficiency of photocatalysts is to increase the concentration of $OH_{surface}$. According to the work of Nakamura,[35] the surface hydroxy groups play two important roles in the photocatalytic reactions. First, the surface hydroxy groups act as hole traps to improve the separation efficiency of electron–

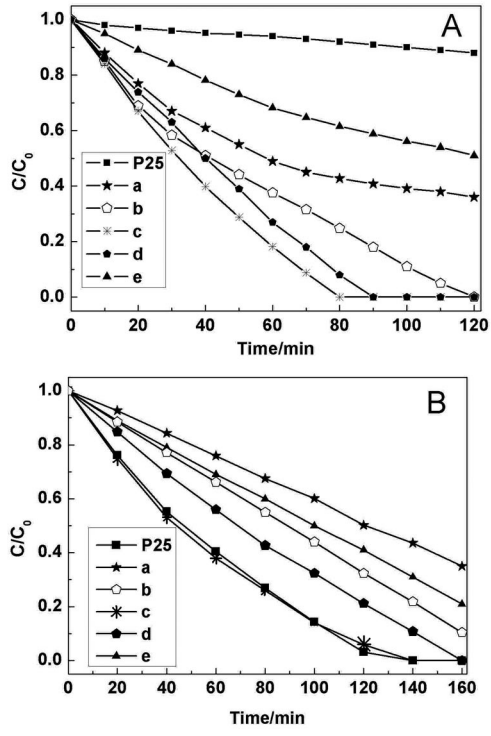

Figure 5. Photocatalytic degradation curves of MB on N-doped TiO_2 samples and P25 (A) under visible light irradiation, (B) under UV irradiation.

hole pairs and to enhance the quantum efficiency. Second, through subsequent reactions, these hydroxy groups can help to form oxidative species with a high activity to mineralize MB. Thus, an increase in the surface hydroxy concentration will lead to enhanced photocatalytic efficiency under both UV and visible light. To inhibit the charge, carrier recombination is an alternative way to enhance the overall quantum efficiency for interfacial charge transfer.[35] It is known that Ti^{3+} can cause the recombination of the trapped electrons with photoholes h^+ ($Ti^{3+} + h^+ \rightarrow Ti^{4+}$). Therefore, a lower concentration of Ti^{3+} sites will lead to a lower recombination rate, a higher separation efficiency of electron–hole pairs, and a higher photocatalytic activity.

Another important route to enhance the quantum efficiency is to stabilize the charge separation through coupling of different crystal phases. Two different models related to stabilization of charge separation by photoinduced interfacial electron transfer have been reported. One is the traditionally accepted model involving the transfer of electrons from anatase to lower-energy rutile electron sites (as mentioned in the introduction for Degussa P25).[21a,21b] Hurum et al. reported another model: under visible-light illumination ($\lambda > 400$ nm), the lower-energy rutile can be irradiated, then rapid electron transfer from rutile to anatase lattice trapping sites will occur in P25.[21c] In the present anatase–brookite mixed-phase system, we take the traditional model and propose that photoinduced interfacial electron transfer from anatase to brookite may also occur. There are mainly two reasons for this: (1) Anatase possess a higher band energy than brookite (3.19 to 3.11 eV)[36] and a higher activity in most cases.[6] (2) Brookite has a higher band energy than rutile (3.11 to 3.0 eV)[36] and is hard to irradiate by visible light. (The band gaps of 3.19, 3.11, and 3.0 eV correspond to the optical absorption edges of 388.7, 398.6, and 413.3 nm.[36])

In addition to quantum efficiency, the visible-light photocatalytic activities of the samples are also related to the component of the chemically bonded N^- species (at 396 eV). The reason is that the N species can serve as active sites for photocatalysis under visible light. Moreover, it should be noted that the BET surface area of the sample also plays an important role for the photocatalytic properties, because a higher specific surface area usually leads to more active sites.

According to the main parameters affecting the photocatalytic degradation process discussed above, the experimental results in the present work are considered to be reasonable. First, N-doping remarkably reduced the band gap energy of TiO_2 materials and, thus, greatly improved photocatalytic activities in the visible-light region for the N-doped samples compared with P25. Second, although the BET surface areas of all five samples with different phase compositions are similar, the band-gap energies and the chemical states of the Ti, O, and N species on the surface of the N-doped TiO_2 samples proved to be tunable by phase mixing of brookite and anatase. Therefore, the photocatalytic activities of the N-doped TiO_2 samples can also be tailored by properly monitoring the phase composition. The highest activity of the bicrystal N-doped TiO_2 catalyst with a phase composition of 24.6%B and 75.4%A (sample c) can be attributed to the relatively higher quantum efficiency and active N^- specie concentration. The higher quantum efficiency may arise from the relatively higher $OH_{surface}$ concentration and the lower number of Ti^{3+} sites. Furthermore, the relatively larger surface areas (compared with P25) and moderate band-gap energy may also contribute to the high activity of sample c.

Conclusions

In summary, the N-doped anatase–brookite bicrystal TiO_2 with acetylacetone as the phase-selective agent was designed and synthesized through a facile solvothermal route. The ratio of the brookite to anatase can be easily tuned by changing the composition of the initial solution. The band-gap energy of the N-doped TiO_2, the chemical states of the Ti, O, and N species on the surface, and the photocatalytic activity of the catalysts were affected by the mixed-phase effect of brookite and anatase. At the optimum ratio of brookite to anatase (24.6 to 75.4%), the N-doped TiO_2 bicrystal catalyst (sample c) exhibits a maximum activity under both visible and UV light. Particularly, the following points should be highlighted: (1) With an in-

crease in the brookite content in the N-doped products, the band-gap energies of the catalysts become wider. (2) The relatively larger surface area (compared with P25) leads to more active sites. (3) The sober mixing of brookite and anatase favors an increase in the concentration of $OH_{surface}$ and a decrease in the number of Ti^{3+} sites, which lead to an increase in quantum efficiency. (4) The mixed-phase catalyst has a maximum concentration of the chemically bonded N^- species (at 396 eV), which serve as active sites for photocatalysis under visible light.

Experimental Section

Synthesis: Tetrabutyltitanate, dimethylformamide (DMF), acetylacetone (acac), and methylene blue (MB) were all analytical grade and purchased from Beijing Chemical Factory. All the N-doped titania samples were synthesized by a single-step solvothermal treatment. In a typical experiment, a certain amount of tetrabutyltitanate, DMF, and acac were mixed (Table 1), then the mixture was transferred into a Teflon-lined autoclave and heated to 180 °C for 48 h. The solid product was filtered, washed, and dried in air at room temperature. The information and the corresponding preparing parameters of five typical samples (identified as samples a, b, c, d, and e) are listed in Table 1.

Catalytic Activity Measurements: The photocatalytic activities of the samples was evaluated by the photodegradation of MB in an aqueous solution at room temperature under ultraviolet and visible light irradiation. In the process, the catalyst (0.09 g) was suspended in a fresh dye aqueous solution (for the UV-induced reaction: $C_0 = 8 \times 10^{-5}$ M; Vis: $C_0 = 4 \times 10^{-6}$ M, 45 mL). The suspension was stirred in the dark for 20 min to allow an adsorption–desorption equilibrium of MB dye. Then oxygen was bubbled into the reactor. After 20 min, the solution was illuminated whilst stirring. At a certain interval, a certain amount of sample (4 mL for the UV-induced reaction, 3 mL for the Vis-induced reaction) was drawn from the system, centrifuged and then the absorption spectrum at 664 nm of the dye was monitored. The UV source was a 100 W mercury lamp ($\lambda > 330$ nm). The visible light irradiation source ($\lambda > 400$ nm) was obtained by putting an appropriate cut-off filter in the front of a 500 W mercury lamp to completely remove wavelengths shorter than 400 nm. The photoreactor was placed on a magnetic stirrer to ensure homogeneous mixing during irradiation.

Characterization: The XRD patterns of the catalysts were recorded with a Rigaku DMAX-2000 X-ray diffractometer by using a Cu-K_α radiation source ($\lambda = 1.54056$ Å). The XRD patterns were used to identify the crystal phase, ratio of anatase to brookite, and crystallite size. The fraction of brookite in the sample was estimated from the following equation:[37]

$$W_B = k_B A_B/(k_A A_A + k_B A_B)$$

where A_A represents the integrated intensity of the anatase (101) peak, and A_B the integrated intensity of brookite (121) peak, and k_A and k_B are two coefficients of anatase and brookite, respectively ($k_A = 0.886$ and $k_B = 2.721$). Due to the overlap of the anatase (101) peak with (120) and (111) of brookite, a numerical deconvolution technique was used to separate these peaks (Figure 6). The XRD intensity of anatase (101) peak at $2\theta = 25.3°$, and brookite (121) peak at $2\theta = 30.8°$ were analyzed. The values of full-width-at-half maximum (FWHM) of the (101) peaks for anatase and (121) peaks for brookite were used to calculate the crystallites size of the samples by Scherrer's equation $D_c = K\lambda/(\beta\cos\theta)$,[38] where D_c, K, λ, β, and θ is the size of crystal, Scherrer constant (0.89), the wavelength of X-ray, FWHM of a selected peak, and diffraction angle for the selected peak, respectively.

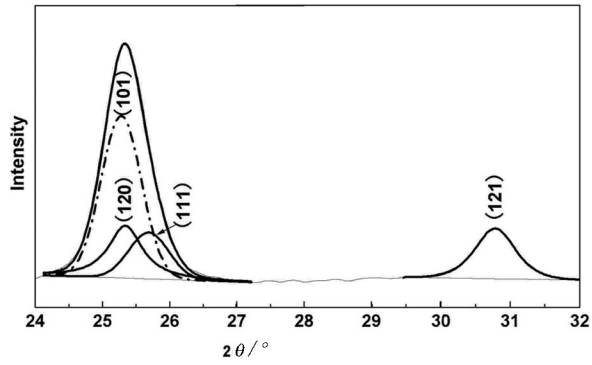

Figure 6. Deconvolution of XRD patterns of sample e in Table 1.

UV/Vis absorption spectra for the dry pressed disk of the samples were obtained by using a UV/Vis spectrophotometer (Varian Cary 5000), which was used to calculate the optical band energy of the samples. Absorption spectra were referenced to $BaSO_4$. TiO_2 is known as an indirect band gap semiconductor, for which the relation between the absorption coefficient and incident photon energy ($h\nu$) can be written as:

$$\alpha \propto (h\nu - E_g)^2/h\nu$$[36,39]

where E_g is the band gap energy of the sample. Plots of $(\alpha h\nu)^{1/2}$ vs. $h\nu$ from the spectroscopic data of Figure 3 is presented in Figure S2. Extrapolating the linear part of the curves give the band gap energy.

XPS measurements were made with a PHI Quantera SXMX spectrometer with an Mg-K_α source (1253.6 eV). The samples are analyzed at pressures less than 10^{-7} Pa. Binding energies were measured for O_{1s}, Ti_{2p}, and N_{1s}. The C_{1s} binding energy of 284.8 eV was taken as the standard for correction of experimental binding energies. The O/Ti/N atomic ratios were also given by the XPS measurements. TEM images were obtained with a JEM-2100F electron microscope.

Supporting Information (see also the footnote on the first page of this article): Detailed SEM images of sample c and P25; illustration for determining the band-gap energies.

Acknowledgments

The authors thank for the support of the 973 Program and the Chinese Academy of Sciences.

[1] P. Pichat, G. Ertl, H. Knözinger, J. Weitkamp, *Handbook of Heterogeneous Catalysis*, **1997**, vol. 4, pp. 2111–2122.
[2] X. Chen, S. S. Mao, *Chem. Rev.* **2007**, *107*, 2891–2959.
[3] A. Fujishima, T. N. Rao, D. A. Tryk, *J. Photochem. Photobiol. C: Photochem. Rev.* **2000**, *1*, 1–21.
[4] O. Carp, C. L. Huisman, A. Reller, *Prog. Solid State Chem.* **2004**, *32*, 33–177.
[5] A. Fujishima, K. Honda, *Nature* **1972**, *238*, 37–38.
[6] M. R. Hoffmann, S. T. Martin, W. Choi, D. W. Bahnemann, *Chem. Rev.* **1995**, *95*, 69–96.
[7] H. Yamashita, Y. Ichihashi, M. Harada, *J. Catal.* **1996**, *158*, 97–101.
[8] E. Piera, J. A. Ayllon, X. Domenech, J. Peral, *Catal. Today* **2002**, *76*, 259–270.

[9] T. Umebayashi, T. Yamaki, H. Itoh, K. Asai, *J. Phys. Chem. Solids* **2002**, *63*, 1909–2002.
[10] D. Dvoranová, V. Brezová, M. Mazúr, M. A. Malati, *Appl. Catal., B* **2002**, *37*, 91–105.
[11] H. Yamashita, M. Harada, J. Misaka, M. Takeuchi, K. Ikeue, M. Anpo, *J. Photochem. Photobiol. A: Chem.* **2002**, *148*, 257–261.
[12] J. K. Zhou, M. Takeuchi, X. S. Zhao, A. K. Ray, M. Anpo, *Catal. Lett.* **2006**, *106*, 67–70.
[13] M. Anpo, *Catal. Surv. Jpn.* **1997**, *1*, 169–179.
[14] R. Asahi, T. Morikawa, T. Ohwaki, K. Aoki, Y. Taga, *Science* **2001**, *293*, 269–271.
[15] S. Sato, *Chem. Phys. Lett.* **1986**, *123*, 126–128.
[16] H. Irie, Y. Watanabe, K. Hashimoto, *J. Phys. Chem. B* **2003**, *107*, 5483–5486.
[17] C. Burda, Y. Lou, X. Chen, A. C. S. Samia, J. Stout, J. L. Gole, *Nano Lett.* **2003**, *3*, 403–409.
[18] H. Li, J. Li, Y. Huo, *J. Phys. Chem. B* **2006**, *110*, 1559–1565.
[19] H. V. Damme, W. K. Hall, *J. Am. Chem. Soc.* **1979**, *101*, 4373–4374.
[20] a) H. Fujii, K. Inata, M. Ohtaki, K. Eguchi, H. Arai, *J. Mater. Sci. Lett.* **1997**, *16*, 1086–1088; b) T. Ozawa, M. Iwasaki, H. Tada, T. Akita, K. Tanaka, S. Ito, *J. Colloid Interface Sci.* **2005**, *281*, 510.
[21] a) T. Kawahara, Y. Konishi, H. Tada, N. Tohge, J. Nishii, S. Ito, *Angew. Chem. Int. Ed.* **2002**, *41*, 2811; b) R. I. Bickley, T. Gonzalez-Carreno, J. S. Lees, L. Palmisano, R. J. D. Tilley, *J. Solid State Chem.* **1991**, *92*, 178; c) D. C. Hurum, K. A. Gray, *J. Phys. Chem. B* **2005**, *109*, 977–980.
[22] a) M. A. Fox, M. T. Dulay, *Chem. Rev.* **1993**, *93*, 341–357; b) A. Hagfeldt, M. Gratzel, *Chem. Rev.* **1995**, *95*, 49–68.
[23] B. Ohtani, J. I. Handa, S. I. Nishimoto, T. Kagiya, *Chem. Phys. Lett.* **1985**, *120*, 292–294.
[24] H. Kominami, M. Kohno, Y. Kera, *J. Mater. Chem.* **2000**, *10*, 1151–1156.
[25] a) X. Chen, C. Burda, *J. Phys. Chem. B* **2004**, *108*, 15446–15449; b) J. L. Gole, J. D. Stout, J. C. Burda, Y. Lou, X. Chen, *J. Phys. Chem. B* **2004**, *108*, 1230–1240; c) E. Gyorgy, P. A. Perezdel, P. Serra, J. L. Morenza, *Surf. Coat. Technol.* **2003**, *173*, 265–270; d) N. C. Saha, H. C. Tomkins, *J. Appl. Phys.* **1992**, *72*, 3072–3079.
[26] a) Y. Chang, J. J. Teo, H. C. Zeng, *Langmuir* **2005**, *21*, 1074–1079; b) J. J. Teo, Y. Chang, H. C. Zeng, *Langmuir* **2006**, *22*, 7369–7377.
[27] G. Q. Li, C. Y. Liu, Y. Liu, *Appl. Surf. Sci.* **2006**, *253*, 2481–2486.
[28] Z. L. Liu, B. Guo, L. Hong, H. X. Jiang, *J. Phys. Chem. Solids* **2005**, *66*, 161–167.
[29] a) H. X. Lin, X. X. Wang, X. Z. Fu, *Prog. Chem.* **2007**, *19*, 665; b) M. A. Henderson, *Langmuir* **1996**, *12*, 5093; c) G. S. Herman, Z. Dohnálek, N. Ruzycki, U. Diebold, *J. Phys. Chem. B* **2003**, *107*, 2788.
[30] X. B. Chen, Y. B. Lou, A. Samia, C. Burda, J. L. Gole, *Adv. Funct. Mater.* **2005**, *15*, 41–49.
[31] J. G. Yu, X. J. Zhao, Q. N. Zhao, J. C. Du, *Chin. J. Mater. Res.* **2000**, *14*, 203–209.
[32] a) S. Sato, *Chem. Phys. Lett.* **1986**, *123*, 126–128; b) H. Irie, Y. Watanabe, K. Hashimoto, *J. Phys. Chem. B* **2003**, *107*, 5483–5486; c) C. Burda, Y. Lou, X. Chen, X. Chen, A. C. S. Samia, J. Stout, J. L. Gole, *Nano Lett.* **2003**, *42*, 403–407.
[33] S. Livraghi, M. C. Paganini, E. Giamello, A. Selloni, C. Di Valentin, G. Pacchioni, *J. Am. Chem. Soc.* **2006**, *128*, 15666–15671.
[34] a) R. K. Wahi, Y. P. Liu, J. C. Falkner, V. L. Colvin, *J. Colloid Interface Sci.* **2006**, *302*, 530.
[35] R. Nakamura, Y. Nakato, *J. Am. Chem. Soc.* **2004**, *126*, 1290–1298.
[36] J. G. Li, T. Ishigaki, X. Sun, *J. Phys. Chem. C* **2007**, *111*, 4969.
[37] H. Zhang, J. F. Banfield, *J. Phys. Chem. B* **2000**, *104*, 3481–3487.
[38] D. E. Gu, B. C. Yang, Y. D. Hu, *Catal. Lett.* **2007**, *118*, 254–259.
[39] a) L. Li, C. Y. Liu, Y. Liu, *Mater. Chem. Phys.* **2009**, *113*, 551–557; b) C. Chao, Z. J. Jiang, C. Y. Liu, *J. Photochem. Photobiol. A: Chem.* **2008**, *195*, 151–155.

Received: April 22, 2009
Published Online: July 21, 2009

